Microstructural, texture, plastic anisotropy and superplasticity development of ZK60 alloy during equal channel angular extrusion processing

E. Mostaed, A. Fabrizi, F. Bonollo, M. Vedani

In this study, equal channel angular pressing (ECAP) was exploited to refine the grain size of a ZK60 magnesium alloy in multi-processing steps, namely at temperatures of 250˚C, 200˚C and 150˚C, producing an ultrafine-grained (UFG) structure. The microstructural development and texture evolution during ECAP were systemically investigated by electron backscattered diffraction (EBSD) analysis. The microstructure of the ECAP processed alloy was remarkably refined to an average grain size of 600 nm. During ECAP process the original fiber texture of the as-extruded alloy was gradually weakened and eventually replaced by a stronger texture component coinciding with ECAP shear plane. The ECAP processed material showed a proper balance of tensile as well as compression strength and tensile ductility at room temperature. Yield strength of 273 and 253 MPa in tension and compression, respectively, ultimate tensile strength of 298 MPa and fracture elongation of about 30% were obtained in the UFG alloy. A transition from ductile–brittle to ductile fracture consisting of very fine and equiaxed dimples was also found in the ECAP processed material. Compared to the as-received alloy, a combination of grain refinement and texture development in the UFG alloy gave rise to a notable reduction in mechanical asymmetric behavior at room temperature. The superplastic behavior of the as-extruded and ECAP processed alloy was also investigated at 200˚C with strain rate of 1.0×10^{-3} s^{-1}. The concurrent effect of grain boundary sliding and favorable basal texture in the UFG alloy led to an achievement of elongation value of about 300% while, under similar testing conditions, the elongation of about 140% was obtained in the as-extruded alloy.

KEYWORDS: ZK60 MG ALLOY - ECAP - ULTRA-FINE GRAIN - TEXTURE - ASYMMETRIC BEHAVIOR - SUPERPLASTICITY

INTRODUCTION

Due to their low density, high specific strength, excellent damping capacity and biocompatibility, magnesium and its alloys have been attracting much attention as potential metallic materials in a wide range of automotive, military, electronic, aerospace and biomedical applications. However, magnesium alloys exhibit poor formability at room temperature due to their hexagonal closed-packed (HCP) crystal structure with limited number of available slip systems [1-5]. In other words, Critical resolved shear stress (CRSS) for a basal slip system {0001} <11$\bar{2}$0> at room temperature is much lower than those of the non-basal slip of <a> type dislocations on prismatic {10$\bar{1}$0} and pyramidal {10$\bar{1}$1} planes. With increasing of temperature, the CRSS of non-basal slip systems decrease gradually, whereas that of basal slip remains constant. Accordingly, non-basal slip mechanisms are responsible for improved ductility of magnesium and its alloys at elevated temperatures [6-8]. Since the non-basal slips were only observed at high temperatures, plastic deformation in polycrystalline Mg alloys appears to be governed entirely by basal slip system at room temperature [9]. As basal plane alone provides only two independent slip systems which are much fewer than those required, five independent slip systems, to fulfill Taylor criterion [10], Mg alloys show poor formability. Hence,

Ehsan Mostaed, Maurizio Vedani
Department of Mechanical Engineering
Politecnico di Milano, Milan - Italy

Alberto Fabrizi, Franco Bonollo
Department of Management and Engineering
Università di Padova
Stradella S. Nicola 3, 36100 Vicenza - Italy

inadequate active deformation systems in such crystal structure gives rise to formation of a strong crystallographic texture upon mechanical processing. Accordingly, mechanical properties of wrought Mg alloys are considerably affected by texture orientation induced by conventional forming processes such as rolling and extrusion [11-13]. However, beside dislocation slip, magnesium represents a strong tendency for twining, especially $\{10\bar{1}2\}\langle 10\bar{1}1\rangle$ extension twin allowing extensive strain parallel to the c-axis. Therefore, twinning in Mg plays a crucial role in plastic deformation upon contribution to meet the Taylor criterion. Moreover, compared to metals with face-centered and body-centered cubic structure, Mg alloys are low-symmetry materials due to possessing low symmetry in their crystal lattice with axial ratios (c/a) of around 1.633 [14,15]. Normally as the axial ratio is less than $\sqrt{3}$, the activation of $\{10\bar{1}2\}\langle 10\bar{1}1\rangle$ extension twin could be achieved by a tensile stress perpendicular to the basal plane or a compressive stress parallel to the basal plane. In other words, the aforementioned twinning is not preferred in tension, while it is favored in compression mode along the extrusion axis. Hence, difference in yield behavior between tension and compression (tension-compression yield asymmetry), restricting Mg alloys from wider applications, is attributed to a dominance of $\{10\bar{1}2\}\langle 10\bar{1}1\rangle$ twinning system [11,16-20]. Nevertheless, previous studies demonstrated that this mechanical asymmetry can be alleviated by several ways such as texture weakening [21,22], alloying elements [23], heat treatment [24] and grain refinement [19,21,22,25].

Superplastic forming of Mg alloys has been proved to play a significant contribution in shaping these materials into complex geometries and curved parts for subsequent use in a wide range of applications such as aerospace and automotive industries [26]. Accordingly, in order to expand their applicability, considerable effort has been devoted to improve the formability as well as yield asymmetry alleviation of wrought Mg alloys.

Superplasticity is a diffusion-controlled process usually occurring at high temperatures (above ~ 0.5 T_m, where T_m is the absolute melting temperature of the material). Furthermore, it requires a small grain size, typically smaller than 10 μm, since the dominant flow process in superplasticity is grain boundary sliding (GBS) [27-29]. Therefore, several studies have been made on tailoring the microstructure through various plastic deformation methods aimed at improving the superplastic ductility.

Thermo-mechanical processing methods such as hot rolling and hot extrusion are used to achieve small grain sizes but generally these approaches cannot be used to attain a grain size smaller than ~2-3 μm. In addition, the mentioned methods generally lead to a strong texture in which the basal planes in most grains are distributed parallel to the rolling or extrusion direction, causing reduction in ductility. It is well known that microstructural refinement induced by severe plastic deformation (SPD) techniques is an effective way for achieving strength and ductility improvement in Mg alloys. As a bulk processing method, equal channel angular pressing (ECAP) is by far one of the most efficient SPD techniques being able to produce metallic materials with uniform distribution of ultra-fine grains, which is believed to be a prerequisite for superplastic behavior through introducing massive strain during deformation [22,30-37].

In this study, an attempt was made to prepare the UFG ZK60 Mg alloy with uniform and equiaxed grain structure through a multi-step ECAP method. The aim of the present work is to systematically investigate the plastic behavior, mechanical asymmetry and superplasticity of UFG and coarse grained alloys at room and high temperatures with the main focus on microstructural and texture evolution induced by ECAP.

EXPERIMENTAL PROCEDURE

Materials and method

In the present work, a commercial ZK60 (Mg-5.3Zn-0.48Zr, wt. %) alloy in the form of extruded bar was selected as a starting material. Cylindrical specimens of 10 mm in diameter with a length of 100 mm were machined from the extruded bars. In this study, as illustrated in Fig. 1, an ECAP die possessing two cylindrical channels of 10 mm in diameter, intersecting at an angle of 110° and with an outer arc of curvature of 20° was used. According to Iwahashi formula [38] this geometry involves an equivalent shear strain of 0.76 on each pass. The whole die was heated by 4 electrical resistance heaters homogeneously distributed around the vertical channel and at the intersection point. ECAP processing, consisted of three steps of deformation, carried out at 250°C, 200°C and 150°C, at which up to 4 passes were performed. Table 1 summarizes the conditions investigated for the ZK60 alloy at the different ECAP temperatures. All the samples were subjected to repetitive pressings and rotated by 90° in the same direction between each pass, according to the procedure designated as route B_C in the literature [39]. Samples were sprayed with MoS_2 lubricant and pressed into the ECAP die at a speed of 30 mm/min.

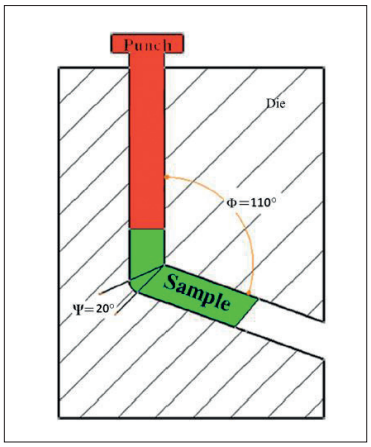

Fig.1 - Schematic illustration of ECAP process.
Illustrazione schematica del processo ECAP

Tab. 1 - ECAP processing conditions of the investigated samples.
Condizioni di processo ECAP dei campioni studiati

Sample code	Sample condition
A	As-extruded ZK60 Mg alloy
E1	ECAP treated for 4 passes at 250°C
E2	E1 + ECAP treated for 4 passes at 200°C
E3	E2 + ECAP treated for 4 passes at 150°C

Microstructural and texture characterization

The microstructures of the all samples were characterized by Electron Backscattered Diffraction (EBSD) technique on the longitudinal plane (the plane containing the two channel axes). In particular, distribution of grain size, crystallographic texture and grain orientation maps of the ZK60 alloy in the as-received condition and after ECAP process were obtained using EBSD technique interfaced with a (FEG-SEM). All the data were then processed with TSL OIM™ software. The typical scan area was 30 μm × 30 μm with a 0.2 μm step size for the ECAP-processed specimen, while, in order to achieve good statistical data due to the presence of coarser grains, a larger scan area was selected for as-received alloy sample. Prior to EBSD analysis, all specimens' surfaces were carefully prepared by standard mechanical polishing followed by low-angle ion milling. The fracture surfaces of all samples at different temperatures of tensile tests were examined using field gun emission scanning electron microscopy (FEG-SEM).

Mechanical characterization

In the present work mechanical properties were evaluated by tensile, compression and Vickers micro-hardness tests. Tensile specimens with a gage length of 12 mm and the diameter of 4 mm were machined along the longitudinal direction of the specimens and tested at room temperature (RT) and 200°C at a strain rate of 1.0×10^{-3} s^{-1}. Compression test was performed at room temperature at a strain rate of 1.0×10^{-3} s^{-1} on cylindrical specimens with a diameter of 10 mm and height of 20 mm, cut along the longitudinal direction from the as-extruded and ECAP processed billets. Micro-hardness measurements were undertaken on the plane parallel to the extrusion and ECAP directions with an indenter load of 1N.

RESULTS AND DISCUSSION

Microstructural and texture characterization

Fig. 2 shows EBSD maps of the investigated samples and the corresponding {0 0 0 2} pole figures, taken on their longitudinal cross-sections. The starting alloy (Fig. 2a) featured a rather heterogeneous and partially recrystallized microstructure with a bimodal grain size distribution of coarse grains along with a large number of fine dynamically recrystallized (DRXed) grains clustered near the band of secondary phase particles (black points). In addition, as seen in Fig. 2a, most of the secondary-phase particles were distributed along the extrusion direction, leading to formation of high-lattice-distortion zones accelerating the DRX process and eventually promoting the grain refinement effect. The microstructure of sample E2 (Fig. 2b) showed a remarkable grain refinement. However, some coarse grains representing the residual part of the original structure are still visible. Eventually, after 4 more passes at 150 °C (sample E3) those remaining grains became refined, leading to an uniform and completely recrystallized microstructure formed by ultra-fine grains of 600 nm average size, as shown in Fig. 2c.

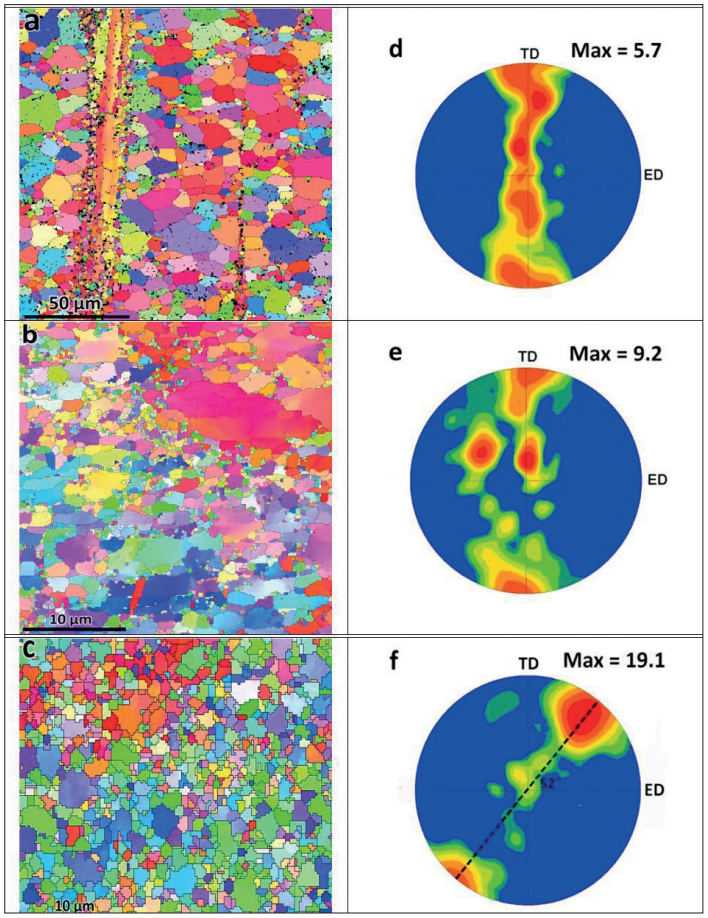

Fig. 2 - Orientation maps and corresponding (0 0 0 2) pole figures of the investigated samples A (a and d), E2 (b and e) and E3 (c and f).
Immagini di orientazione e corrispondenti figure polari del piano (0002) dei campioni studiati A (a,d), E2 (b,e), E3 (e,f)

Fig. 2d reveals that sample A exhibited a typical extrusion texture, with (0 0 0 2) planes oriented parallel to extrusion direction (ED). As ECAP processing advanced to E2 sample, the prevailing texture with basal planes parallel to ED weakened although a stronger component with basal planes parallel to the ED still remained (Fig 2e) so that the typical texture of E2 sample is somewhat similar to the initial fiber texture. However, the maximum texture intensity increased from 5.7 to 9.2 as sample A underwent two steps of ECAP processing (E2).

Subsequent step of ECAP (sample E3) fully replaced the original fiber texture by a newly formed texture component with basal planes preferentially tilted by 52° to the processing direction (Fig. 2f), implying that the majority of grains have an orientation favorable for dislocation glide on the dominant slip plane (0002) and, moreover, the maximum texture intensity increased up to 19.1. In short, it should be noted that the original fiber texture, whereby higher tensile strength along ED is achieved, was progressively disintegrated and finally substituted by a new dominant texture developed at E3 condition.

Table 2 summerizes the mean values of Schmid factors for {0001} <11$\bar{2}$0> basal slip system in the as-extruded and ECAP processed samples. It can be observed that with accumulation of ECAP passes, the value of Schmid factor on basal planes consistently increased, leading to a significant improvement from 0.17 to 0.30 for A and E3 samples, respectively.

It is well known that in pure Mg at room temperature, the critical resolved shear stress (CRSS) of the basal slip system is 100 times lower than that of non-basal slip systems. That is, at room and moderately elevated temperatures, plastic deformation is mostly governed by the basal slip system since other slip systems can hardly be activated [40,41].

Thus, the maximum Schmid factor for basal slip can be achieved when basal planes are oriented with an angle of 45° to the stress axis.

It is worth mentioning that for Mg and its alloys the orientation between basal plane and the applied stress axis is of major importance from the mechanical point of view, especially in terms of tensile strength and fracture elongation [31].

Accordingly, the increment in Schmid factor value by ECAP progress (higher value of 0.30 for E3 condition) brings about the substantial improvement in alloy's ductility. In short, as the Schmid factor on (0 0 0 1) basal planes increases by the rotation of the basal planes to approximately close to the theoretical ECAP shear plane, a lower stress is needed for yielding on the basal plane in the UFG sample.

Tab. 2 - Schmid factor values for basal slip in the investigated samples.
Fattore di Schmid relativo al piano basale dei campioni studiati

Sample condition	Schmid factor for basal slip
A	0.17
E2	0.24
E3	0.30

MECHANICAL CHARACTERIZATION

Micro-hardness

Fig. 3 represents the Vickers micro-hardness variations of the ZK60 alloy measured on longitudinal sections (LS) of the as-received and ECAP processed samples. For sample A, the hardness value on longitudinal section (67.5 HV) was higher than that measured on the transversal plane (63.7 HV), which is attributed to an intense texture inherited from extrusion, with the majority of the basal planes lying parallel to the extrusion direction, causing the generation of {10$\bar{1}$2} <10$\bar{1}$1> twins [42]. From the general trend it is clearly seen that, by increasing the number of ECAP passes, the hardness of the alloy raises. Furthermore, the gap in hardness values between LS and TS progressively degraded, insinuating that E3 sample shows more isotropic behavior.

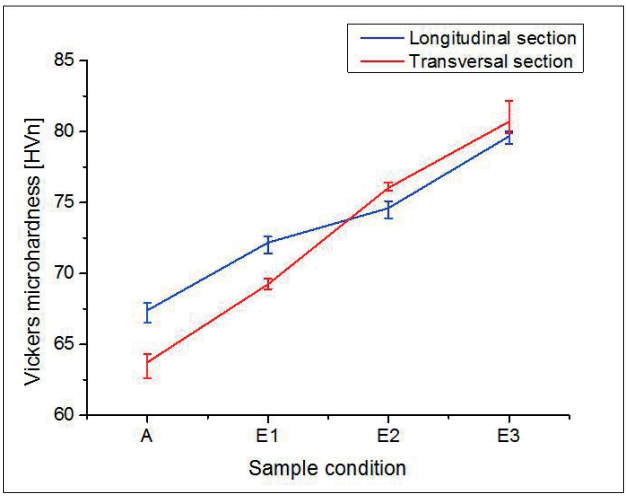

Fig. 3 - Hardness evolution as a function of sample condition.
Evoluzione della durezza al variare della condizione dei campioni

Tensile properties

Fig. 4. shows the mechanical asymmetry expressed by the ratio of tensile to compression yield stress as a function of samples condition.

Sample A showed relatively high asymmetric ratio of about 1.8 which is associated with the activation of the {10$\bar{1}$2} <10$\bar{1}$1> twins during the compression while the load axis was parallel to the basal planes. However, the aforementioned twin could not be active in tension mode. Thus, the TYS was significantly higher than the measured CYS in the as extruded condition. Based on previous reports, when the grains become finer, basal and non-basal slip and even grain boundary sliding mechanisms can be active and, thereby, suppress the twinning during the deformation. Moreover, twinning is more likely to occur in bigger grains. With advancement of ECAP process since the strong basal plane fiber extrusion texture (Fig. 2f) gradually degraded and it is eventually substituted by a new one according to which the basal planes were oriented close to the theoretical ECAP shear plane, the ratio of tensile to compression yield stress gradually decreased and finally for E3 sample it reached about 1.1, implying that the UFG sample showed an isotropic mechanical behavior in both tension and compression.

The 0.2% proof stress in tension (TYS), ultimate tensile strength

(UTS) and tensile fracture elongation (FE) obtained from tensile and compressive stress versus strain curves are plotted in Fig. 4b. It should be noted that very similar shapes of stress-strain curves were obtained from the repeated tensile testing, indicating that the scatter of the mechanical testing data in the present study is small because the tensile specimens were taken in the homogeneously deformed central region of the ECAPed samples. Considering that the grain structure was substantially refined with increasing number of ECAP passes and due to decreasing temperature, a progressive rise in tensile strength would be expected. Nevertheless, UTS and TYS decrease form 339 and 290 MPa to 308 and 216 MPa, respectively.

Therefore, factors other than grain size should be considered in the present case to account for the observed trend. The decrease of obtained TYS and UTS values is mainly attributed to the weakening of the initial fiber texture (Fig. 2d and e) by increasing the texture intensity and also the Schmid factor from 5.7 and 0.17 to 9.2 and 0.24, respectively.

Accordingly, the texture modification played a dominant role in the first two steps and it compensates for grain refining strengthening effect, leading to a decrease in both TYS and UTS. Further ECAP passes (E3) led to a meaningful TYS improvement, up to 273 MPa, that was also accompanied by higher fracture ductility (TE of about 30%). In other words, the texture softening effect is stronger than the strengthening effect given by grain refining by ECAP.

Considerable improvement in both strength and fracture elongation obtained in E3 sample can be explained by two distinct observations. First, as stated, a uniform and equiaxed ultra-fine grained microstructure with grain size of 600 nm was achieved in E3 sample (Fig. 2c).

Hence, according to the Hall-Petch relationship, the TYS of E3 is expected to be higher than that of the previous condition (E2). Furthermore, the formation of a newly introduced shear texture with a higher maximum texture intensity accompanied by activation of non-basal slip systems due to grain boundary compatibility stress [43] both induced a significant improvement of FE of about 30%. In short, in the case of E3 sample, a combination of grain refinement and texture development is responsible for improved combination of strength and ductility.

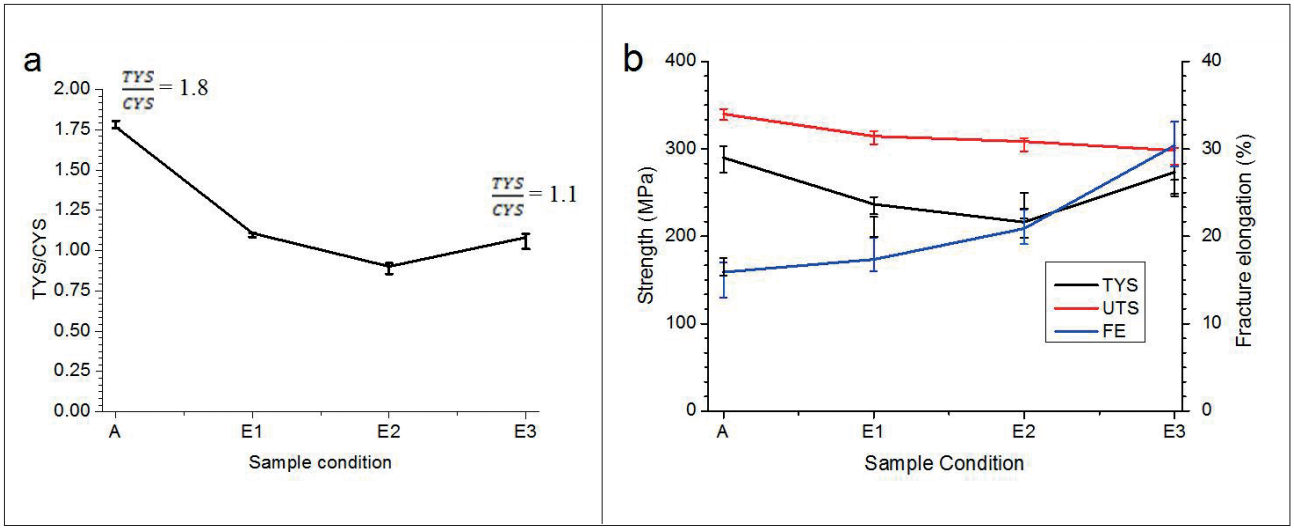

Fig. 4 - The dependence of (a) yielding asymmetry and (b) mechanical properties on samples conditions.
Dipendenza della asimmetria del carico di snervamento (a) e delle proprietà meccaniche in generale (b) dalle condizioni dei campioni studiati

Fig. 5a shows the curves of true stress versus true strain obtained at a stable temperature of 200°C and at the strain rate of $1.0 \times 10^{-3}s^{-1}$. As apparent, the curve of sample E3 includes a lower strain hardening and high elongations to failure. The flow stress dropped significantly even though higher ductility was then achieved. The significant difference in the flow stress of A and E3 alloys can be attributed to the textural softening of the ECAPed condition, similar to that operating at room temperature, while the marked improvement of elongation is supposed to be strongly related to the deformation mechanisms of grain boundary sliding (GBS) [27,28]. In other words considerable grain size reduction by ECAP also provided higher superplastic elongation. The ability to achieve superplasticity at lower temperatures is an important consideration if the alloy is utilized commercially in superplastic forming operations.

General Views of the specimens strained to failure are shown in Fig.5b where the upper specimen is in the untested condition. As seen, the specimen exhibited a maximum elongation of about 300%, implying a general thinning of the deforming material in a very uniform fashion rather than initiating a necking phenomenon which is typically observed in more conventional coarse-grained metals. Tensile failure in an uniform manner without the development of local necking is a characteristic feature of superplastic flow [44].

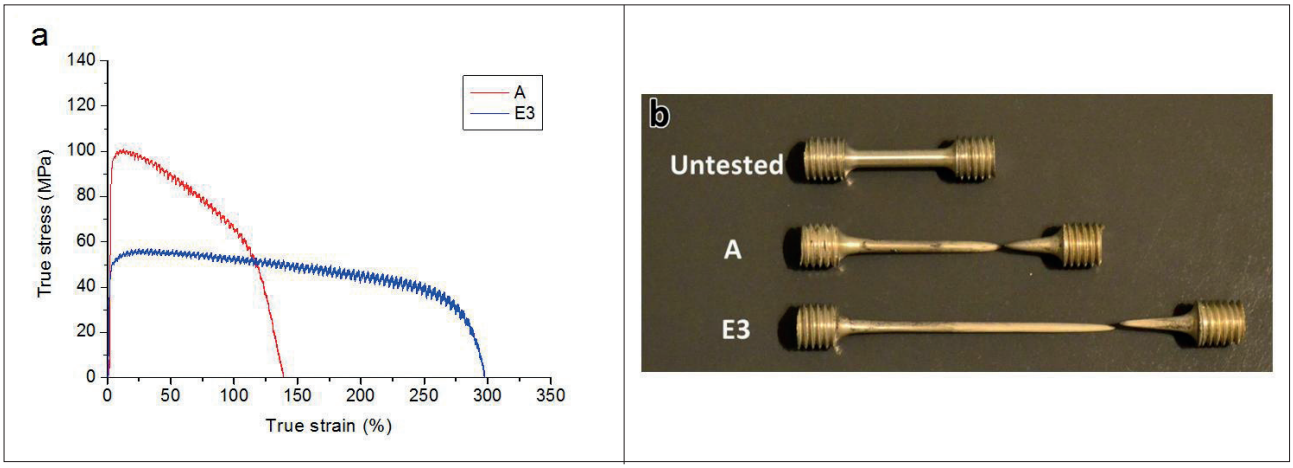

Fig. 5 - (a) True stress vs. true strain curves recorded at 200°C and strain rate of 1.0×10^{-3} s^{-1} for A and E3 samples (b) general appearance of the samples deformed to fracture.
(a) curve sforzo vero - deformazione naturale registrate a 200°C e ad una velocità di deformazione di 1.0×10-3 s-1 per i campioni A ed E3; aspetto generale dei campioni deformati a frattura.

Fractography

Fig.6 reveals SEM representative fractographs of samples A and E3 at RT and 200°C. It can be seen from Fig.6a that a large number of dimples and cleavage planes are visible on the fracture surface, suggesting that sample A experienced a mixed ductile-brittle fracture mode. In contrast, Fig.6b shows the E3 sample fracture surface with considerably larger fraction of very fine and equiaxed dimples, which are almost uniform in size separated by sharp ridges, representing the typical features of markedly ductile fracture behavior. At temperature of 200°C the number of observed dimples on the fracture surface of A sample increased consistently (Fig. 6c) and they also became deeper with various size distribution arising from the initial bimodal grain structure (as seen in Fig. 2a). The size of the dimples is strongly related to the size of the material's grains since it is dependent on the initiation site and the number of voids nucleated at the grain boundaries [45]. Accordingly, as seen in Fig. 6d, after ECAP (E3) the fracture surface was almost completely covered by small size plastic dimples, resulting from uniform equiaxed grain structure generated by ECAP, indicating high obtained tensile elongation of 300%.

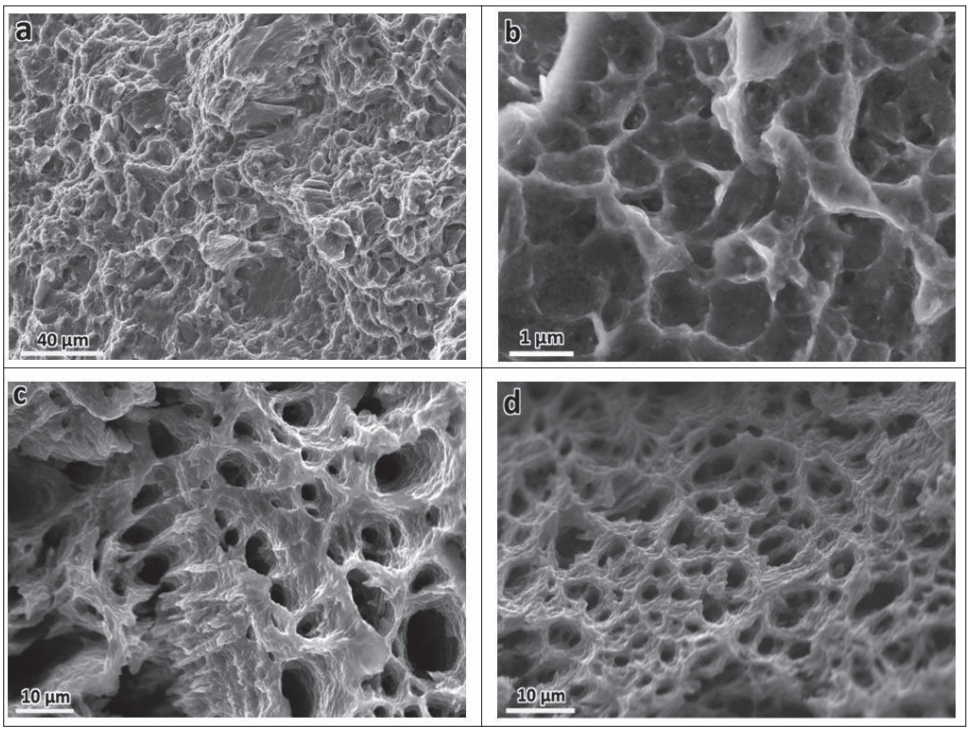

Fig. 6 - SEM micrographs of fractured tensile specimens at room temperature (a) A, (b) E3 and at 200°C (c) A and (d) E3.
Micrografie SEM dei provini fratturati in trazione a temperatura ambiente (a) A, (b) E3 e A a 200°C (c,d)

CONCLUSION

In this study ZK60 Mg alloy was subjected to ECAP aimed at obtaining ultra-fine grained (UFG) structure. The effect of such a structure on mechanical properties, plastic anisotropy and superplasticity was investigated. The following conclusions can be drawn from this research work:

1 - The coarse grained microstructure of the as-extruded samples was substituted by a homogeneous equiaxed ultra-fine grained structure with 600 nm average size through ECAP processing. After several ECAP passes saturation of properties was achieved.

2 - The texture investigation demonstrated that the initial fiber texture of ZK60 extruded alloy was progressively undermined during first two ECAP steps. Afterwards, at the final step of the process (150°C), the fiber texture was replaced by a newly stronger texture component featuring basal planes preferentially aligned along the theoretical ECAP shear plane with higher maximum texture intensity and Schmid factor values.

3 - Mechanical anisotropy in UFG sample was significantly reduced due to remarkable grain refinement as well as the activation of non-basal slip systems at the UFG scale.

4 - Microstructural, texture and mechanical characterization revealed that a combination of grain refinement and texture development led to an improvement of both strength and ductility in UFG sample condition. In other words, markedly improvement in elongation to failure of about 100% was obtained while keeping relatively high tensile strength.

5 - The UFG alloy exhibited excellent superplastic properties after processing by ECAP, leading to a considerable failure elongation in tension of 300% at 200°C when using a strain rate of 1.0×10^{-3} s^{-1}. By comparison, the equivalent elongation in the extruded condition without ECAP was about 140%.

REFERENCES

[1] B.L. Mordike, T. Ebert, Magnesium: Properties - applications - potential, Mater. Sci. Eng. A. 302 (2001) 37-45. doi:10.1016/S0921-5093(00)01351-4.

[2] Y. Chino, K. Kimura, M. Mabuchi, Twinning behavior and deformation mechanisms of extruded AZ31 Mg alloy, Mater. Sci. Eng. A. 486 (2008) 481-488. doi:10.1016/j.msea.2007.09.058.

[3] S.E. Ion, F.J. Humphreys, S.H. White, Dynamic recrystallisation and the development of microstructure during the high temperature deformation of magnesium, Acta Metall. 30 (1982) 1909-1919. doi:10.1016/0001-6160(82)90031-1.

[4] E. Mostaed, M. Vedani, M. Hashempour, M. Bestetti, Influence of ECAP process on mechanical and corrosion properties of pure Mg and ZK60 magnesium alloy for biodegradable stent applications, Biomatter. 4 (2014) e28283.

[5] F. Witte, N. Hort, C. Vogt, S. Cohen, K.U. Kainer, R. Willumeit, et al., Degradable biomaterials based on magnesium corrosion, Curr. Opin. Solid State Mater. Sci. 12 (2008) 63-72. doi:10.1016/j.cossms.2009.04.001.

[6] B.C. Wonsiewicz, Plasticity of magnesium crystals., Thesis, Massachusetts Institute of Technology, 1966. http://dspace.mit.edu/handle/1721.1/27989 (accessed March 9, 2014).

[7] C. Bettles, M. Barnett, Introduction, in: C. Bettles, M. Barnett (Eds.), Adv. Wrought Magnes. Alloys, Woodhead Publishing, 2012: pp. xii-xiii. http://www.sciencedirect.com/science/article/pii/B978184569968050017X (accessed September 7, 2014).

[8] B. Srinivasarao, N.V. Dudamell, M.T. Pérez-Prado, Texture analysis of the effect of non-basal slip systems on the dynamic recrystallization of the Mg alloy AZ31, Mater. Charact. 75 (2013) 101-107. doi:10.1016/j.matchar.2012.10.002.

[9] T. Obara, H. Yoshinga, S. Morozumi, {1122} <1123> Slip system in magnesium, Acta Metall. 21 (1973) 845-853. doi:10.1016/0001-6160(73)90141-7.

[10] S.G.I. Taylor, Plastic Strain in metals, 1938.

[11] S. Kleiner, P.J. Uggowitzer, Mechanical anisotropy of extruded Mg-6% Al-1% Zn alloy, Mater. Sci. Eng. A. 379 (2004) 258-263. doi:10.1016/j.msea.2004.02.020.

[12] G. Garcés, P. Pérez, P. Adeva, Effect of the extrusion texture on the mechanical behaviour of Mg-SiCp composites, Scr. Mater. 52 (2005) 615-619. doi:10.1016/j.scriptamat.2004.11.024.

[13] A. Prakash, S.M. Weygand, H. Riedel, Modeling the evolution of texture and grain shape in Mg alloy AZ31 using the crystal plasticity finite element method, Comput. Mater. Sci. 45 (2009) 744-750. doi:10.1016/j.commatsci.2008.06.015.

[14] M.M. Avedesian, H. Baker, A.I.H. Committee, Magnesium and magnesium alloys, ASM International, 1999.

[15] S.X. Song, J.A. Horton, N.J. Kim, T.G. Nieh, Deformation behavior of a twin-roll-cast Mg-6Zn-0.5Mn-0.3Cu-0.02Zr alloy at intermediate temperatures, Scr. Mater. 56 (2007) 393-395. doi:10.1016/j.scriptamat.2006.10.040.

[16] E.A. Ball, P.B. Prangnell, Tensile-compressive yield asymmetries in high strength wrought magnesium alloys, Scr. Metall. Mater. 31 (1994) 111-116. doi:10.1016/0956-716X(94)90159-7.

[17] Y.N. Wang, J.C. Huang, The role of twinning and untwinning in yielding behavior in hot-extruded Mg-Al-Zn alloy, Acta Mater. 55 (2007) 897-905. doi:10.1016/j.actamat.2006.09.010.

[18] J. Bohlen, M.R. Nürnberg, J.W. Senn, D. Letzig, S.R. Agnew, The texture and anisotropy of magnesium-zinc-rare earth alloy sheets, Acta Mater. 55 (2007) 2101-2112. doi:10.1016/j.actamat.2006.11.013.

[19] L.L. Chang, Y.N. Wang, X. Zhao, M. Qi, Grain size and texture effect on compression behavior of hot-extruded Mg-3Al-1Zn alloys at room temperature, Mater. Charact. 60 (2009) 991-994. doi:10.1016/j.matchar.2009.04.001.

[20] S.R. Agnew, M.H. Yoo, C.N. Tomé, Application of texture simulation to understanding mechanical behavior of Mg and solid solution alloys containing Li or Y, Acta Mater. 49 (2001) 4277-4289. doi:10.1016/S1359-6454(01)00297-X.

[21] S.M. Yin, C.H. Wang, Y.D. Diao, S.D. Wu, S.X. Li, Influence of Grain Size and Texture on the Yield Asymmetry of Mg-3Al-1Zn Alloy, J. Mater. Sci. Technol. 27 (2011) 29-34. doi:10.1016/S1005-0302(11)60021-2.

[22] E. Mostaed, M. Hashempour, A. Fabrizi, D. Dellasega, M. Bestetti, F. Bonollo, et al., Microstructure, texture evolution, mechanical properties and corrosion behavior of ECAP processed ZK60 magnesium alloy for biodegradable applications, J. Mech. Behav. Biomed. Mater. (n.d.). doi:10.1016/j.jmbbm.2014.05.024.

[23] J. Bohlen, P. Dobroň, J. Swiostek, D. Letzig, F. Chmelík, P. Lukáč, et al., On the influence of the grain size and solute content on the AE response of magnesium alloys tested in tension and compression, Mater. Sci. Eng. A. 462 (2007) 302-306. doi:10.1016/j.msea.2006.02.470.

[24] J. Jain, W.J. Poole, C.W. Sinclair, M.A. Gharghouri, Reducing the tension-compression yield asymmetry in a Mg-8Al-0.5Zn alloy via precipitation, Scr. Mater. 62 (2010) 301-304. doi:10.1016/j.scriptamat.2009.11.024.

[25] D.L. Yin, J.T. Wang, J.Q. Liu, X. Zhao, On tension-compression yield asymmetry in an extruded Mg-3Al-1Zn alloy, J. Alloys Compd. 478 (2009) 789-795. doi:10.1016/j.jallcom.2008.12.033.

[26] A.J. Barnes, Superplastic Forming 40 Years and Still Growing, J. Mater. Eng. Perform. 16 (2007) 440-454. doi:10.1007/s11665-007-9076-5.

[27] T.G. Langdon, The mechanical properties of superplastic materials, Metall. Trans. A. 13 (1982) 689-701. doi:10.1007/BF02642383.

[28] T.G. Langdon, An evaluation of the strain contributed by grain boundary sliding in superplasticity, Mater. Sci. Eng. A. 174 (1994) 225-230. doi:10.1016/0921-5093(94)91092-8.

[29] E. Mostaed, A. Fabrizi, D. Dellasega, F. Bonollo, M. Vedani, Microstructure, mechanical behavior and low temperature superplasticity of ECAP processed ZM21 Mg alloy, J. Alloys Compd. 638 (2015) 267-276. doi:10.1016/j.jallcom.2015.03.029.

[30] T. Mukai, M. Yamanoi, H. Watanabe, K. Higashi, Ductility enhancement in AZ31 magnesium alloy by controlling its grain structure, Scr. Mater. 45 (2001) 89-94. doi:10.1016/S1359-6462(01)00996-4.

[31] S.R. Agnew, J.A. Horton, T.M. Lillo, D.W. Brown, Enhanced ductility in strongly textured magnesium produced by equal channel angular processing, Scr. Mater. 50 (2004) 377-381. doi:10.1016/j.scriptamat.2003.10.006.

[32] M. Eddahbi, P. Pérez, M.A. Monge, G. Garcés, R. Pareja, P. Adeva, Microstructural characterization of an extruded Mg-Ni-Y-RE alloy processed by equal channel angular extrusion, J. Alloys Compd. 473 (2009) 79-86. doi:10.1016/j.jallcom.2008.05.064.

[33] R.B. Figueiredo, T.G. Langdon, Principles of grain refinement and superplastic flow in magnesium alloys processed by ECAP, Mater. Sci. Eng. A. 501 (2009) 105-114. doi:10.1016/j.msea.2008.09.058.

[34] G.B. Hamu, D. Eliezer, L. Wagner, The relation between severe plastic deformation microstructure and corrosion behavior of AZ31 magnesium alloy, J. Alloys Compd. 468 (2009) 222-229. doi:10.1016/j.jallcom.2008.01.084.

[35] Y. Ogushi, E. Mostaed, D. Dellasega, M. Vedani, H. Miyamoto, H. Fujiwara, Aging behavior of ECAP processed AZ80 Mg alloy, IOP Conf. Ser. Mater. Sci. Eng. 63 (2014) 012076. doi:10.1088/1757-899X/63/1/012076.

[36] E. Mostaed, Q. Ge, M. Vedani, P.A. De Oliveira Botelho, C. Zanella, F. Deflorian, Investigation on the influence of grain size on strength, ductility, and corrosion properties in Mg and Mg-Zn based alloys for biodegradable stents, Eur. Cell. Mater. 26 (2013) 84.

[37] A. Bussiba, A. Ben Artzy, A. Shtechman, S. Ifergan, M. Kupiec, Grain refinement of AZ31 and ZK60 Mg alloys - towards superplasticity studies, Mater. Sci. Eng. A. 302 (2001) 56-62. doi:10.1016/S0921-5093(00)01354-X.

[38] Y. Iwahashi, J. Wang, Z. Horita, M. Nemoto, T.G. Langdon, Principle of equal-channel angular pressing for the processing of ultra-fine grained materials, Scr. Mater. 35 (1996) 143-146. doi:10.1016/1359-6462(96)00107-8.

[39] V.M. Segal, Equal channel angular extrusion: from macromechanics to structure formation, Mater. Sci. Eng. A. 271 (1999) 322-333. doi:10.1016/S0921-5093(99)00248-8.

[40] W.B. Hutchinson, M.R. Barnett, Effective values of critical resolved shear stress for slip in polycrystalline magnesium and other hcp metals, Scr. Mater. 63 (2010) 737-740. doi:10.1016/j.scriptamat.2010.05.047.

[41] K. Máthis, K. Nyilas, A. Axt, I. Dragomir-Cernatescu, T. Ungár, P. Lukáč, The evolution of non-basal dislocations as a function of deformation temperature in pure magnesium determined by X-ray diffraction, Acta Mater. 52 (2004) 2889-2894. doi:10.1016/j.actamat.2004.02.034.

[42] Y. Chino, K. Kimura, M. Hakamada, M. Mabuchi, Mechanical anisotropy due to twinning in an extruded AZ31 Mg alloy, Mater. Sci. Eng. A. 485 (2008) 311-317. doi:10.1016/j.msea.2007.07.076.

[43] J. Koike, T. Kobayashi, T. Mukai, H. Watanabe, M. Suzuki, K. Maruyama, et al., The activity of non-basal slip systems and dynamic recovery at room temperature in fine-grained AZ31B magnesium alloys, Acta Mater. 51 (2003) 2055-2065. doi:10.1016/S1359-6454(03)00005-3.

[44] T.G. Langdon, Fracture processes in superplastic flow, Met. Sci. 16 (1982) 175-183. doi:10.1179/030634582790427208.

[45] M.-H. Cai, C.-Y. Lee, Y.-K. Lee, Effect of grain size on tensile properties of fine-grained metastable β titanium alloys fabricated by stress-induced martensite and its reverse transformations, Scr. Mater. 66 (2012) 606-609. doi:10.1016/j.scriptamat.2012.01.015.